Investigation of a Monotropic Liquid Crystal Polyurethane Based on Biphenol, 2,6-Tolylene Diisocyanate, and a Six Methylene Containing Flexible Spacer. 1. Thermal and Structure Characterization

Fotios Papadimitrakopoulos, Shaw L. Hsu,* and William J. MacKnight*

Department of Polymer Science and Engineering, University of Massachusetts, Amherst, Massachusetts 01003

Received September 24, 1991; Revised Manuscript Received April 13, 1992

ABSTRACT: The structure and phase behavior of a polyurethane (2,6-LCPU-6) based on the mesogenic biphenol 4,4′-bis(6-hydroxyhexoxy)biphenyl (BHHBP) and 2,6-tolylene diisocyanate (2,6-TDI) have been investigated by differential scanning calorimetry (DSC), polarized optical microscopy, and wide-angle X-ray scattering (WAXS). The isotropic to mesophase transition is approximately 60–70 °C lower than the crystal melting transition. Rapid cooling (faster than 100 °C/min) is necessary to observe the mesophase. Soxhlet extraction in hot MeOH increases considerably the orientation as well as the perfection of mesophase fibers without transforming them to the thermodynamically more stable crystal phase. The mesophase of 2,6-LCPU-6 has a layer thickness of ca. 58 Å and is contracted more than 12 Å from the fully extended conformation. The meta-substituted TDI ring introduces a backbone "kink" which results in a zigzag structure. The mesophase is of higher order than smectic C and has a centrosymmetric structure that leads to a particularly intense 004 layer reflection. Polarized optical microscopy studies demonstrate that 2,6-LCPU-6 exhibits two macroscopically distinct crystal morphologies—a spherulitic morphology produced from slow cooling and a threaded crystalline morphology produced upon heating from the quenched mesophase.

Introduction

Thermotropic liquid crystalline polymers with alternating rigid and flexible units along the backbone have drawn considerable attention. The synthesis and characterization of these polymers are well documented in numerous reviews.[1-3] Thermotropic liquid crystal polyesters, polyethers, polycarbonates, etc., have been shown to form stable liquid crystalline phases over a wide range of temperatures. However, the liquid crystallinity of mesogenic containing polyurethanes is still a subject of debate. The lack of detailed structural characterization and their poor thermal stability above 200 °C[4,5] are the principal reasons for the uncertainties that exist. Previous studies[6-9] indicate that mesogenic polyurethanes rarely exhibit stable mesophases. Characterization of those mesogenic polyurethanes which melt without significant decomposition[6-8a,8c,9a] suggests their monotropic[1,14,15] liquid crystalline nature. Although quite extensive thermal analysis, polarizing optical microscopy, and spectroscopic methods have been used in order to elucidate various aspects of the structure of these material, wide-angle X-ray scattering (WAXS) has not been fully utilized. In particular the polyurethane designated as 2,4-LCPU-6 has received

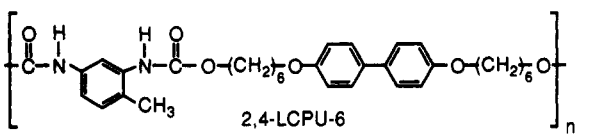

considerable attention[6,7,10-13] from our laboratory. It has been shown that 2,4-LCPU-6 forms a monotropic liquid crystal phase of a smectic C type. Further, it has a strong tendency to crystallize despite the presence of the "asymmetric" methyl group on the 2,4-tolylene diisocyanate (2,4-TDI) moiety. The *N*-methyl analogue of 2,4-LCPU-6, NM-2,4-LCPU-6, exhibits a stable smectic C mesophase[7] but no stable crystal phase. Comparison of NM-2,4-LCPU-6 and 2,4-LCPU-6 reveals that H bonding is of only secondary importance in determining mesophase formation and morphology.

In this paper, we will describe the synthesis, thermal analysis, optical microscopy, and WAXS characterization of the polyurethane designated 2,6-LCPU-6. The sym-

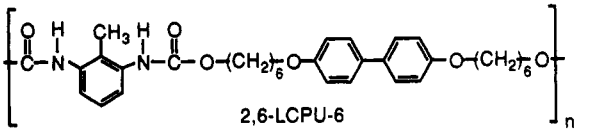

metrically placed methyl group in the 2,6-tolylene diisocyanate (2,6-TDI) affords a comparison between its phase behavior and that of 2,4-LCPU-6. As will become apparent in the discussion, the randomly substituted methyl group along the polymer chain of 2,4-LCPU-6 leads to a lowering of the transition temperatures[1,2] and the "partial" stabilization of the mesophase relative to the crystal phase. However the unsymmetrical methyl group complicates molecular modeling and crystallographic analysis.[16-21] Fortunately the transition temperatures of 2,6-LCPU-6 are within the acceptable limits of polyurethane thermal stability.[4,5]

The present paper is the first of a series devoted to a detailed investigation of various aspects of the structure and phase behavior of 2,6-LCPU-6. We will attempt to obtain a molecular understanding of the structure and phase transitions of 2,6-LCPU-6. This will in turn lead to a fundamental assessment of the roles of the mesogen, the hydrogen bonding, and the placement of the methyl group in the TDI in governing the phase behavior in these monotropic liquid crystalline polyurethanes.[22]

Experimental Section

Materials. All chemicals were obtained from Aldrich. The reaction solvents were dried and distilled before their use, and recrystallization solvents were stored previously over activated 3–4-Å molecular sieves. Prepurified Ar and N_2 inert gases were previously passed over BTS catalyst (O_2 scavenger)[23] and $CaCl_2$ desiccant. *N,N*-Dimethylformamide (DMF) was stirred over BaO for 2 days, at room temperature, filtered with a 0.45-μm syringe filter to remove residual BaO, and vacuum distilled at ~30 mmHg

0024-9297/92/2225-4671$03.00/0

Scheme I

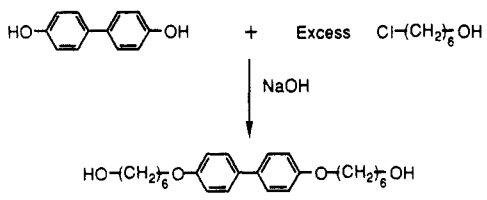

BHHBP

and the middle portion was kept. The 2,6-TDI was vacuum distilled at ~0.5 mmHg, and the middle portion was kept.

Mesogenic Diol (BHHBP). The synthesis of 4,4'-bis(6-hydroxyhexoxy)biphenyl (BHHBP) is indicated in Scheme I and has been described in detail previously.[6,7] We report for the first time the ^{1}H NMR data of BHHBP. ^{1}H NMR (DMF-d_7) (reported as follows: chemical shift (Both chemical shifts of doublets are reported. Only the middle peak, chemical shift of triplets of pentates is reported. Chemical shifts of multiplets are reported from the higher to lower), multiplicity, integration, assignment in Figure 1): δ 7.94/7.91 (d, 4 H, a), 7.40/7.37 (d, 4 H, b), 4.74 (t, 2 H, h) 4.39 (t, 4 H, g), 3.84 (t, 4 H, c), 2.16 (p, 4 H, f), 1.97–1.56 (m, 12 H, e + d).

Preparation of the Mesogenic Polyurethane (2,6-LCPU-6) (Scheme II). The 2,6-LCPU-6 polyurethane was synthesized by the reaction of BHHBP and 2,6-TDI. A slight excess (0.3–0.7 mol %) of 2,6-TDI was used to compensate for side reactions involving isocyanate groups. The reaction was run on several scales, ranging from 3 to 20 g. Higher molecular weights were obtained in the larger scale polymerizations, probably because the influence of impurities was decreased. The procedure described here is for the small-scale preparation whereas for the larger scale, which produced the highest molecular weight, the excess 2,6-TDI was 0.5 mol %.

Into a 250-mL flame-dried, three-neck, round-bottom flask fitted with a condenser, pressure equalizing dropping funnel, inert gas inlet, and magnetic stirrer were added 4.8035 g (12.428 mmol) of Diol-6 and 50 mL of freshly distilled DMF. Purified Ar was bubbled through the solution for 15 min, and its temperature was raised to 45 °C. Argon was kept flowing slowly through the top of the apparatus continually. Subsequently, 2.1709 g (12.465 mmol) of freshly distilled 2,6-TDI (0.3% excess) and 30 mL of DMF were added slowly. The temperature was raised slowly to 85 °C and held there for 20 h. As the reaction proceeded, 20 mL more of DMF was added to keep the solution viscosity low enough to allow stirring. Finally the reaction temperature was raised to 95 °C, held there for an additional 12 h, and cooled to 45 °C. The warm, viscous solution was poured into cold filtered MeOH to precipitate the polymer in the form of white, fibrous material. The polymer was filtered, Soxhlet extracted in hot MeOH, and vacuum dried to give 6.6 g of 2,6-LCPU-6 (yield 94.3%), $[\eta]$ = 0.400 dL/g. ^{1}H NMR (DMSO-d_6) (reported, in order, as chemical shift, multiplicity, integration, assignment in Figure 1): δ 8.88 (s, 2 H, h), 7.50/7.47 (d, 4 H, a), 7.09 (s, 3 H, j + k), 6.96/6.93 (d, 4 H, b), 4.03 (t, 4 H, g), 3.95 (t, 4 H, c), 2.02 (s, 3 H, i), 1.75–1.65 (br s, 4 H, f), 1.65–1.55 (br s, 4 H, d), 1.5–1.3 (br s, 8 H, e). Elemental Anal. Calcd for $C_{33}H_{40}N_2O_6$: C, 70.69; H, 7.19; N, 5.00. Found: C, 70.68; H, 7.30; N, 4.95.

Characterization Techniques. Intrinsic viscosities were determined in 1,1,1,3,3,3-hexafluoro-2-propanol 99+% (HFIP; Aldrich) at 30.0 °C and in DMF at 70.0 °C, using a Cannon–Ubbelohde viscometer. Elevated temperatures were employed to ensure complete solubilization.

Solution ^{1}H NMR spectra were recorded on a Varian XL-300 operating at 300 MHz in deuterated solvents. All spectra were referenced relative to the solvent chemical shifts.

Optical microscopy was performed on a Carl Zeiss Ultraphoto II polarizing microscope equipped with a Linkham Scientific Instruments TMS 90 temperature controller and a TMH 600 hot stage. The hot stage temperature was calibrated with vanillin and potassium nitrate melting point standards.

Differential scanning calorimetric (DSC) measurements were conducted with a Perkin-Elmer DSC-7, employing a 20 mL/min flow of dry nitrogen as a purge gas for the sample and reference cells. The coolant was ice–water except for the case of the rapid-cooling experiments where chopped dry ice was employed. The temperature and power ordinates of the DSC were calibrated with respect to the known melting point and heat of fusion of a high-purity indium standard. Long-term annealing was performed under nitrogen or vacuum to ensure the absence of oxidative thermal degradation.

Room-temperature X-ray diffraction patterns were recorded on flat films with a Statton X-ray camera using Ni-filtered Cu Kα radiation. The samples, free-standing fibers or contained in 1.5-mm Lindemann glass tubes, were mounted directly on the pinhole with the help of double-stick tape. The X-ray camera length was calibrated with the 2.319-Å diffraction line of NaF and 3.035-Å diffraction line of $CaCO_3$ for the wide-angle range, while for the intermediate-angle range, the layer diffraction lines of the monoclinic form of n-hexatriacontane, n-$C_{36}H_{74}$[25] was used. The films were measured for interplanar spacing data with a Supper circular film measuring device. Well-oriented samples were produced by drawing fibers out of the melt, with a pair of tweezers. Free-standing fibers were exposed to thermal and Soxhlet treatment in MeOH, while a weight of 0.5–3 g was attached to their ends in order to prevent shrinkage. No significant elongation was observed after the end of each treatment.

Results and Discussion

Molecular Weight Characterization. The 2,6-LCPU-6 is soluble in polar aprotic solvents such as DMF, DMAC, DMSO, etc., only at elevated temperatures (above 70 °C). Hexafluoro-2-propanol (HFIP) was found capable of solubilizing 2,6-LCPU-6 at room temperature, without significant molecular weight degradation. Intrinsic viscosity measurements were performed in HFIP (at 30.0 °C) as well as in DMF (at 70 °C). Molecular weight determination by means of gel permeation chromatography (GPC) was not possible due to the insolubility of 2,6-LCPU-6 in polar aprotic solvents (at room temperature). In the present study two samples of 2,6-LCPU-6 were employed. The polymer referred to as low molecular weight was determined to have an intrinsic viscosity of 0.400 dL/g and the polymer referred to as high molecular weight had an intrinsic viscosity of 0.882 dL/g. From the intrinsic viscosity measurements it is apparent that a reasonably high degree of polymerization has been achieved.

Differential Scanning Calorimetry. Typical 10 °C/min heating and cooling traces of 2,6-LCPU-6 are illustrated in Figure 2.

For the low molecular weight polymer (Figure 2A), upon heating, a weak step in heat capacity corresponding to the glass transition (T_g) is observed at approximately 65–85 °C. This is followed by a broad shallow exotherm, typical of "cold crystallization", with a peak at ~160 °C. This region of exothermic behavior is typically more intense on the first heating scan than subsequently. In addition, a strong endotherm with a peak at 190 °C, followed by a weaker one with a peak at 197 °C, is also observed. The overall ΔH_m from 139 to 209 °C is 42.0 ± 0.5 J/g. Upon cooling, a sharp exotherm around 158 °C followed by a 25 °C exothermic "tail" is observed. The overall ΔH_c from 126 to 166 °C is 41.6 ± 0.5 J/g.

For the high molecular weight polymer (Figure 2B), upon heating, the T_g is observed at approximately 65–85 °C. This is also followed by a very weak cold crystallization region, with a peak at ~160 °C. Endothermic behavior similar to but slightly broader than that of the low molecular weight polymer is also observed. The strong endotherm peaks at 190 °C and the weak one at 197 °C. The overall ΔH_m from 139 to 209 °C is 41.4 ± 0.5 J/g. Upon cooling, the sharp exotherm is observed at 151 °C, 7 °C lower than in the low molecular weight 2,6-LCPU-6. The

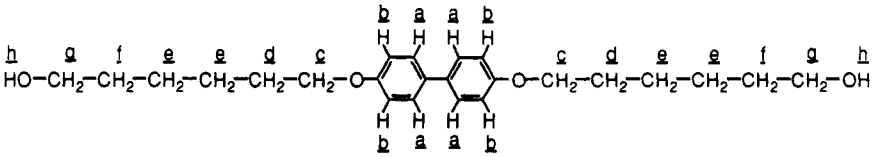

BHHBP

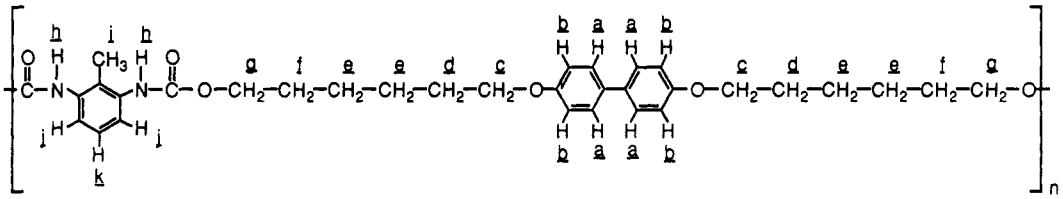

2,6-LCPU-6

Figure 1. Structures of BHHBP and 2,6-LCPU-6. Lower case letters refer to ^{1}H NMR results (see Experimental Section).

Scheme II

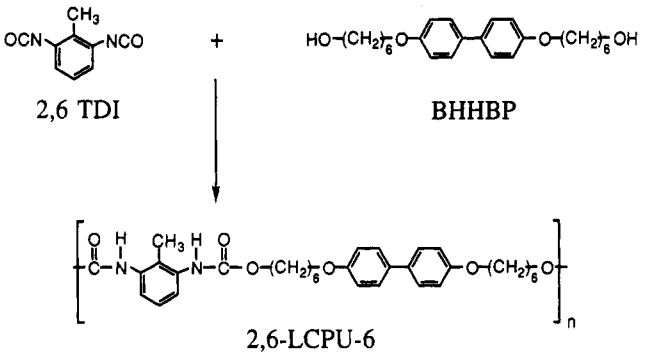

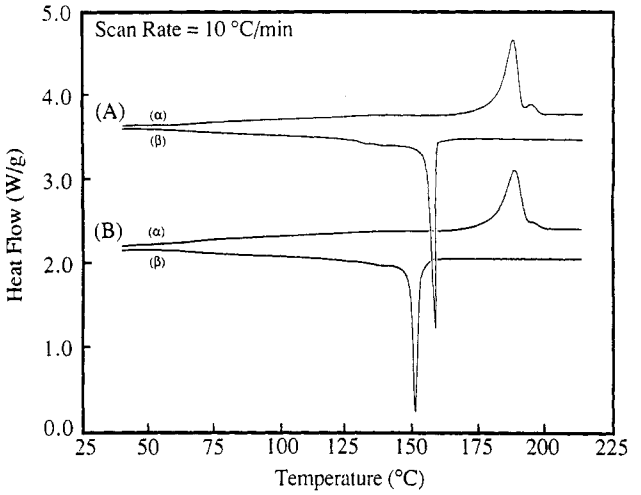

Figure 2. DSC traces for (A) low molecular weight 2,6-LCPU-6 and (B) high molecular weight 2,6-LCPU-6 recorded at 10 °C/min scanning rate: (α) heating; (β) cooling curves.

exothermic tail of this sharp exotherm extends for 15–20 °C, in a fashion similar to the corresponding exotherm in the low molecular weight polymer. The overall ΔH_c from 115 to 162 °C is 41.8 ± 0.5 J/g.

It is apparent that the high molecular weight sample exhibit thermal behavior which is very similar to that of the low molecular weight sample, with the exception of the sharp exothermic peak, on the cooling scan. Particular attention was given to ensure complete isotropization of the two samples, in order to destroy residual crystallinity that might act as crystallization nuclei. This was accomplished by heating the molten samples 2–3 min at elevated temperatures (210–225 °C) before the subsequent cooling

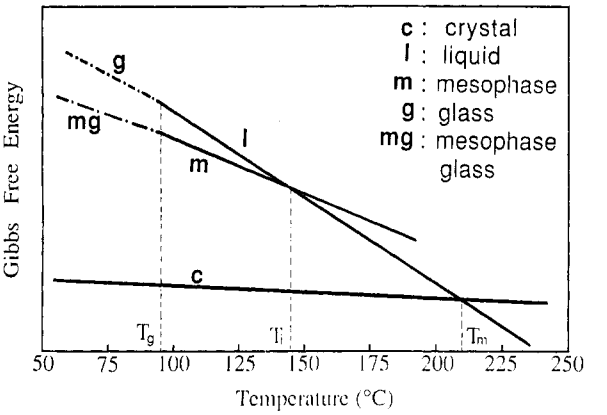

Figure 3. Schematic plot of temperature dependence of Gibbs free energy for 2,6-LCPU-6 (see text for details).

scan. In addition, moisture levels were kept very low by storing the samples in vacuum desiccators before and after successive measurements. Although the urethane bond is known to undergo a variety of reactions above 200 °C,[4,5] almost no changes were observed in the time frame of this experiment apart from a slight yellowing of the samples. Therefore the reason for this 7 °C difference in their sharp exothermic transition temperatures upon cooling must arise from the molecular weight difference which affects the mobility of the polymers and the concentration of end groups.

The monotropic liquid crystalline phase behavior of 2,4-LCPU-6 is well established.[6] The randomly substituted methyl group along the polymer chain of 2,4-LCPU-6 somewhat destabilizes the crystalline phase and makes the mesophase easier to observe. In the case of 2,6-LCPU-6, the methyl group is symmetrically placed along the polymer backbone, leading to a more stable crystal phase than in the case of 2,4-LCPU-6.[14] Having this model in mind, we will undertake the task of explaining most of the features of the 2,6-LCPU-6 polymer. A schematic plot of the temperature dependence of Gibbs free energy (Figure 3) is a convenient way to express the relative thermodynamic stability of the crystalline, liquid crystalline, and liquid phases. The solid lines in Figure 3 represent the equilibrium temperature dependence of each phase. (Note that each sample can be a composite of many individual phases.) Polymers in particular often exhibit marked kinetic effects in the vicinity of the equilibrium phase transitions. Supercooling is very common because of the high viscosity of such systems. In particular, polymers

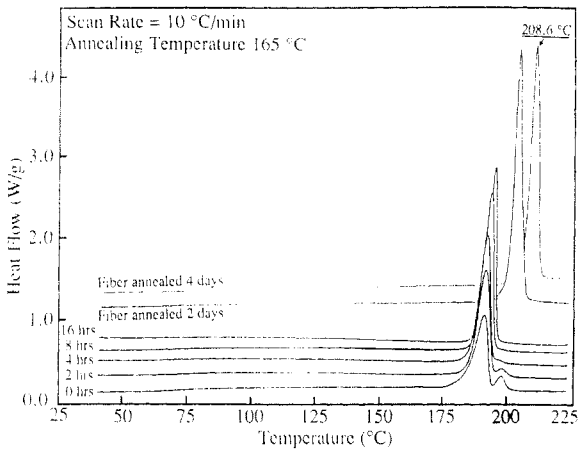

Figure 4. DSC heating traces of high molecular weight 2,6-LCPU-6 samples, previously annealed at 165 °C for various annealing times.

usually crystallize with a large degree of supercooling.[28b] On the other hand, mesophase formation generally requires less supercooling.[29] Thus it is possible to observe a mesophase formation upon cooling 2,6-LCPU-6 rapidly from the melt, without the occurrence of crystallinity. The accessibility of the mesophase is easily seen to be a function of the cooling rate.

Annealing at 165 °C, 5 °C higher than the peak of the shallow cold crystallization region, has proven to be an effective way to increase the crystallinity of 2,6-LCPU-6. The 10 °C/min heating traces of the high molecular weight 2,6-LCPU-6, previously annealed at 165 °C for various times, are presented in Figure 4. The strong endothermic peak at 190 °C is gradually transformed into a single, much sharper endotherm with a higher T_m and ΔH_m. On the other hand, the weaker endotherm at 197 °C gradually decreases in the annealing process and eventually disappears into the rising lower temperature, strong endotherm. Similar behavior is also observed for the low molecular weight sample. As will be discussed in the following papers of this series, WAXS indicates the existence of only one crystal structure which is subjected to perfection and densification upon annealing. This explains the gradual shift of the 190 °C peak toward higher temperatures but does not address the nature of the 197 °C peak. Examination by means of polarizing optical microscopy reveals unambiguously the existence of two different crystalline domains with different morphologies. The two domains melt at temperatures very near to the DSC melting points and have volume ratios comparable to the DSC transition enthalpies. Previous thermal investigations[6] of 2,4-LCPU-6 also disclosed multiple endotherms on melting, which were explained similarly. The 10 °C/min DSC heating scans for two fiber samples were incorporated into Figure 4 to indicate the amount of crystal perfection that can be achieved by orientation and long-term annealing. The fiber annealed for 4 days shows a melting point of 208.6 °C and $\Delta H_m = 69.8$ J/g, ~1.7 times greater than the overall ΔH_m of Figure 2B. It is noteworthy that the 208.6 °C peak can be higher than the equilibrium melting point due to superheating phenomena.[28c] Following publications will address in detail the development of crystallinity in the 2,6-LCPU-6 system.

The effect of cooling rate on the exothermic processes that occur on cooling is illustrated in Figure 5 for the low molecular weight 2,6-LCPU-6. Complete isotropization was ensured by preheating the sample to 225 °C for 2 min and holding the temperature at 210 °C for an additional 1 min before the start of the cooling scan. At the end of each cooling scan the sample was replaced with a fresh one and the old one was subjected to WAXS for further phase characterization. From Figure 5 it is observed that as the scanning rate is increased the main peak at 160 °C shifts to lower temperatures and broadens. In addition a smaller peak at ~133 °C is observed at the end of the exothermic tail. Table I lists the transition temperatures and enthalpies for the cooling scans of Figure 5. The main peak shifts to lower temperatures 3 times faster than the smaller one. From a simple deconvolution of the two peaks the enthalpy under the small peak increases at the expense of the main peak. Similar behavior has been observed for the high molecular weight 2,6-LCPU-6 as well. Before any decisive conclusion about the nature of these peaks is drawn, it is necessary to take WAXS data into consideration.

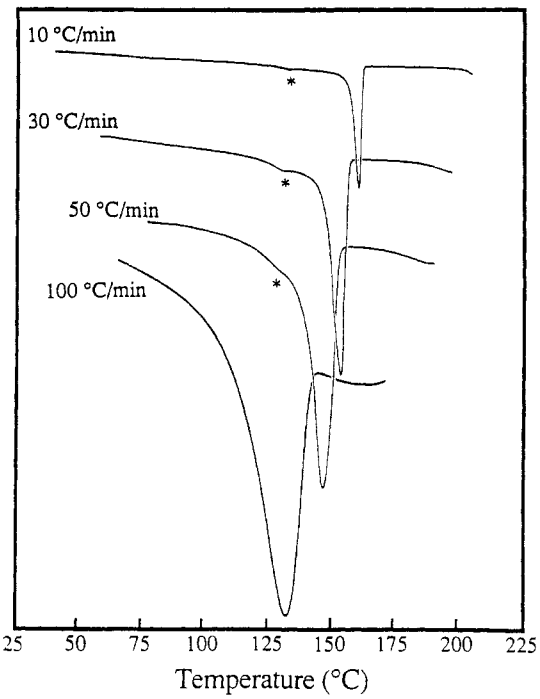

Figure 5. DSC cooling traces of the low molecular weight 2,6-LCPU-6 for various cooling rates.

Table I
Differential Scanning Calorimetric Data for the Low Molecular Weight 2,6-LCPU-6 as a Function of Cooling Rate

cooling rate, °C/min	transition temp, °C		total transition enthalpy, ΔH_c, J/g·min	rel % transition enthalpy[c]	
	T_c[a]	T_c[b]		ΔH_c[a]	ΔH_c[b]
10	160	133	42	95	5
30	153	131	41	92.5	7.5
50	147	129	40	8.9×10	1.1×10
100	132		39		

[a] Main exothermic peak in Figure 5. [b] Smaller peak at the end of the exothermic tail, indicated with an asterisk in Figure 5. [c] Estimated from a simple deconvolution.

X-ray Diffraction. Powder Samples. All X-ray diffraction patterns of powder samples were obtained at room temperature, which is ~50 °C lower than the glass transition temperature of 2,6-LCPU-6. The desired thermal history was imposed on the samples either in a sealed DSC pan or in a temperature-controlled vacuum oven. The samples were cooled rapidly to room temperature after the heat treatment. Figure 6 presents the X-ray powder pattern of the low molecular weight 2,6-LCPU-6 sample, cooled at 100 °C/min from the melt to room temperature (from Figure 5). As will become apparent in

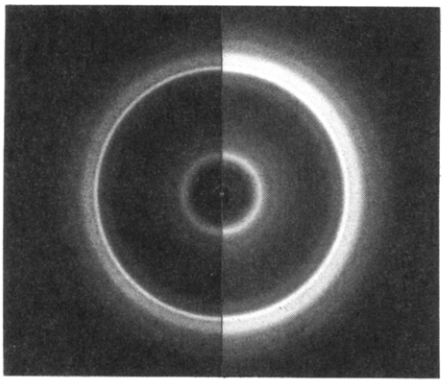

Figure 6. Room-temperature X-ray diffraction powder pattern of a low molecular weight 2,6-LCPU-6 sample, cooled 100 °C/min from the melt to the room temperature (underexposed, left half; overexposed, right half).

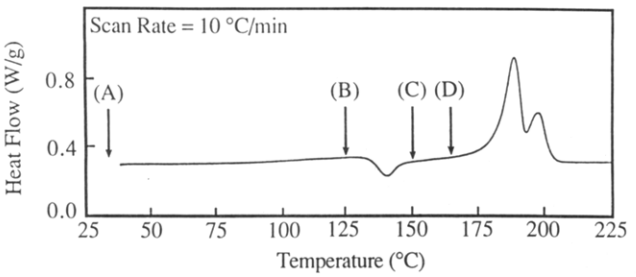

Figure 7. DSC heating trace of a high molecular weight 2,6-LCPU-6 sample quenched into liquid N_2 from the melt.

the discussion, the eight well-defined rings of Figure 6 powder pattern manifest the crystalline character of this sample. Slightly better resolved X-ray powder patterns have been obtained from the other samples of Figure 5, which have been cooled more slowly. Similar behavior has been observed for the high molecular weight 2,6-LCPU-6 as well.

From the above DSC experiments it is obvious that these cooling rates are not sufficient to uncover the mesophase if it exists. Liquid N_2 quenching can be an effective method of providing low levels of contamination as well as cooling rates in the range of thousands of degrees per minute. Figure 7 illustrates a typical 10 °C/min heating trace of a high molecular weight 2,6-LCPU-6 sample quenched into liquid N_2 from the melt (225 °C). The exotherm peaking at 140 °C is the important feature in this DSC heating scan. The ΔH under this exotherm, measured from 127 to 157 °C, is 5.8 J/g, corresponding to a $\Delta S = 1.4 \times 10^{-2}$ J/g·K. In addition, the two well-separated endotherms, peaking at 189 and 197 °C, appear in the same positions as their counterparts from Figure 2. It is noteworthy to mention that the overall ΔH_m from 127 to 207 °C is 41.5 J/g, almost identical with its counterpart from Figure 2 (41.4 ± 0.5 J/g).

In order to characterize the 140 °C exotherm, X-ray powder patterns were taken above and below it. Figure 8 presents the room-temperature X-ray powder patterns of four high molecular weight 2,6-LCPU-6 DSC samples with the following thermal history. All four samples were quenched in liquid N_2 from the melt and allowed to return slowly to room temperature, where the WAXS powder pattern of sample A was obtained. Samples B and C were subjected to 10 °C/min heating scans, to 125 and 150 °C, respectively, and cooled at 100 °C/min to room temperature. Sample D was subjected to a 10 °C/min heating scan, to 165 °C, maintained isothermally at this temperature for 90 min, and then cooled at 100 °C/min to room temperature. Even a brief examination of the (A) and (B) WAXS powder patterns (4–6 rings) serves to confirm their different structures as compared to those of (C) and (D) (8–12 rings). In fact the C and D patterns of Figure 8 are identical with the crystalline WAXS powder pattern of Figure 6.

The X-ray patterns of Figure 8A and B exhibit three inner sharp rings corresponding to the lattice spacings given in Table II and III, respectively. These three sharp reflections can be indexed, within experimental error, as even orders of a 57.6- and 58.2-Å spacings, respectively, indicating a strong layer ordering of biphenyls and TDI electron-rich moieties as well as a small fiber axis expansion with increase of temperature. (The odd-order reflections are extremely weak and can be observed at highly overexposed, oriented samples. In particular, the first-order reflection is the strongest of all odd-order reflections and has been observed from medium small-angle X-ray scattering diffraction of fiber patterns at 54 Å.) In addition to the three sharp inner reflections, there are a few broad reflections that constitute the outer part of the Figure 8A and B powder pattern associated with the weak intermolecular lateral ordering. The strong diffuse halo centered at a spacing of 4.5 Å followed by the well-defined outer ring at 4.0 Å indicates a higher than smectic A or C mesophase but lower than the higher order smectics such as B, G, etc.[34] From the powder pattern alone, we were unable to characterize the type of mesophase present. Therefore it was necessary to obtain highly oriented fiber patterns in order to assess that problem.

The slight expansion of the chain repeat (from 57.6 to 58.2 Å) and the small contraction of the well-defined outer ring (from 4.05 to 4.00 Å) implies an underlying lateral ordering process in the mesophase. The ordering is greatly enhanced above 140 °C, where the mesophase to crystal transformation occurs. This is manifested by the increase in the number of reflections at the wide angles and the smearing of the 002 and 004 as well as the disappearance of the 008 layer reflection. The behavior of the 002 and 004 reflections suggests that the chain repeat continues to expand (58.4 Å for the 8C and 58.7 Å for the 8D powder pattern) and reaches a length 1.1 Å longer than that of the quenched mesophase after annealing at 165 °C for 90 min.

The remarkable sharpness of the main exotherm upon cooling has drawn considerable attention during the course of this investigation (Figures 2 and 4). Even though it appears to be an isotropic to mesophase transition, X-ray analysis suggests that the final form of the sample at room temperature is crystalline. The good agreement of transition enthalpies in the 10 °C/min DSC scans of Figures 2, 5, and 7, along with the assumption that the same amount of 2,6-LCPU-6 is always involved in the transitions schematically depicted in Figure 3, can provide us with a rough understanding of the magnitude of the isotropic–mesophase transition. Figure 7 indicates that the mesophase–crystal transition ($\Delta H_{lc-c} = 5.8$ J/g) is 14% relative to the crystal–isotropic transition ($\Delta H_{c-i} = 41.5$ J/g). If the above assumption is correct, the isotropic–mesophase transition must account for the remaining 86% ($\Delta H_{c-i} = 35.7$ J/g), indicative of a strong order in the mesophase. We deliberately ignore the enthalpy of cold crystallization for reasons of simplicity, since its contribution is very small. These arguments along with the very small transition enthalpy under the lower temperature exotherm (~5% relative to ΔH_{c-i}, Table I) contribute to the composite character of the main exotherm.

Smyth et al.,[6] in their study on low molecular weight 2,4-LCPU-6, observed that the main exothermic transition shifts to higher temperatures with slower cooling rates.

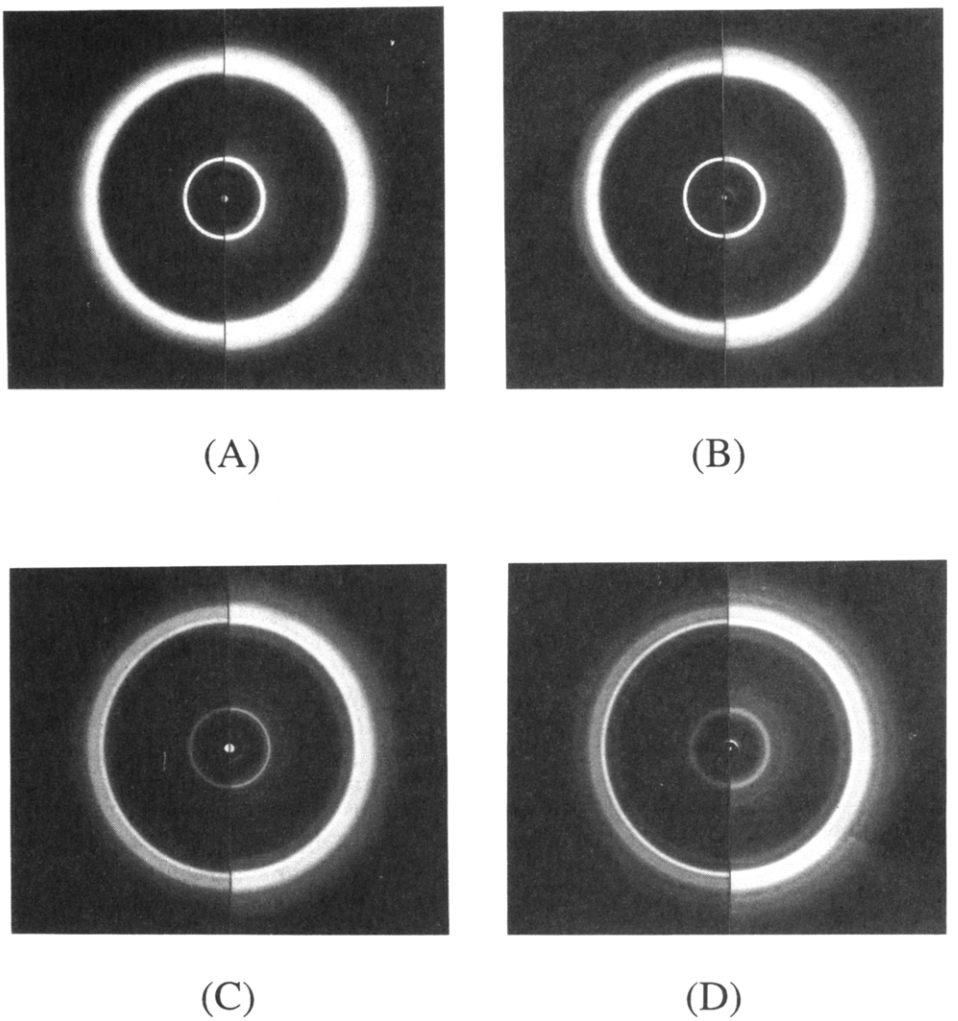

Figure 8. Room-temperature X-ray diffraction powder patterns of high molecular weight 2,6-LCPU-6 samples which have been quenched in liquid N_2 from the melt, heated 10 °C/min to (B) 125 °C, (C) 150 °C, and (D) 165 °C and kept for 90 min at 165 °C (see letters in Figure 7), and cooled 100 °C/min to room temperature (underexposed, left half; overexposed, right half).

Table II
Observed and Calculated *d* Spacings of Figure 8A X-ray Powder Pattern, Indexed as Orders of 57.6 Å

d_{obsd}, Å	intensity	orders of 57.6 Å	d_{calcd}, Å
28.8	weak, sharp	2	28.8
14.34	very strong, sharp	4	14.40
		6	9.60
7.20	weak, sharp	8	7.20
4.5	strong, broad		
4.05	medium, wd[a]		
3.3	very weak, broad		

[a] Well distinguished.

Table III
Observed and Calculated *d* Spacings of Figure 8B X-ray Powder Pattern, Indexed as Orders of 58.2 Å

d_{obsd}, Å	intensity	orders of 58.2 Å	d_{calcd}, Å
29.0	weak, sharp	2	29.1
14.55	very strong, sharp	4	14.55
		6	9.70
7.28	weak, sharp	8	7.28
4.5	strong, broad		
4.00	medium, wd[a]		
3.3	very weak, broad		

[a] Well distinguished.

They presented enough arguments to support the conclusion that at low cooling rates the two-stage exothermic process (isotropic to mesophase, followed by the mesophase to crystal transition) is replaced by a single-stage exothermic process, which is remarkably sharp and narrow. Similarly in 2,6-LCPU-6, because crystallization occurs so fast and readily, a 10–50 °C/min cooling rate can be considered low. Therefore, due to its higher mobility, the low molecular weight sample crystallizes faster (7 °C higher) than the high molecular weight one. Although a single-stage exothermic process which involves crystallization of the sample explains the behavior upon cooling of the main exotherm, it fails to address the nature of the lower temperature exotherm. The stabilized mesophase from copolymers of 2,4-TDI and 2,6-TDI with BHHBP[35] indicates that the isotropic to mesophase transition occurs in the vicinity of 130 °C. With this in mind we can propose the following scenario to elucidate the lower temperature exotherm. As the cooling rate increases, there is less time left for the ordered domain to "space fill" the sample as well as to perfect itself, leaving more and more sample liquidlike. When the temperature is around 130 °C the liquidlike portions convert to mesophase.

To demonstrate even further the involvement of crystallization in the main exotherm upon cooling, we examined the 10 °C/min DSC behavior of a sample annealed at 165 °C for 4 days (Figure 9). Stenhouse et al.[11] observed a molecular weight dispersity of 1.42 and 1.87 for their fresh 2,4-LCPU-6 samples. Because there is very little difference in the way 2,4-LCPU-6 and 2,6-LCPU-6 were synthesized, it is reasonable to assume the polydispersity of fresh 2,6-

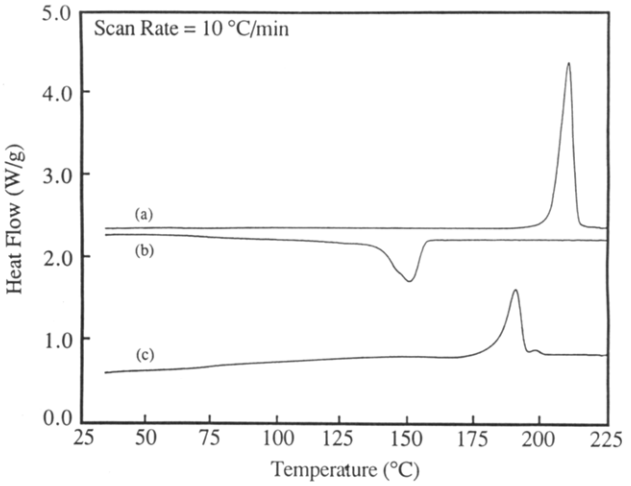

Figure 9. DSC traces of a high molecular weight 2,6-LCPU-6 sample previously annealed at 165 °C for 4 days: (a) first heating; (b) first cooling; (c) second heating.

LCPU-6 to be comparable to that of the 2,4-LCPU-6. On the other hand, the polydispersity of the sample annealed for 4 days at 165 °C is expected to be much higher than 2, due to the well-documented transurethanefication as well as other side reactions[4,5] occurring at this elevated temperature. Figure 9 shows, as expected, that the molecular weight distribution affects only the cooling trace (9b) while the second heating trace (9c) is virtually identical to that of Figure 2Bα. On the first heating we observe the sharp crystal melting endotherm at 210 °C (ΔH_m = 72.8 J/g). The first cooling trace shows a "typical" broad crystallization exotherm peaking at 150 °C (ΔH_c = 40.5 J/g), 1 °C lower than the sharp crystallization peak of Figure 2Bα. This "textbook" behavior of polydispersity upon crystallization[28b] proves unequivocally the involvement of crystallization in the main exotherm upon cooling. On second heating, the typical cold crystallization region around 160 °C is followed by a strong exotherm peaking at 190 °C and a weaker one peaking at 197 °C ($\Delta H_{m(144-210)}$ = 40.0 J/g). This shows that very little has changed in the sample apart from the polydispersity and a 3% reduction of the crystallization transition enthalpy.

X-ray Diffraction, Oriented Samples. It is difficult to obtain well-oriented samples of normal polyurethanes primarily due to their low molecular weights. Blackwell et al.[19] employed a polyurethane hard-segment-rich thermoplastic elastomer (slowly stretched in water to ~700%, and annealed for 24 h at 130 °C) in order to get the desired orientation.

The slow relaxation rate of liquid crystalline polymers is a great advantage in obtaining highly oriented samples. The maximum molecular orientation we were able to accomplish, drawing fibers of high molecular weight 2,6-LCPU-6 from the melt, is demonstrated in Figure 10. As shown in Figure 10, there are two basic features to note: (1) a series of meridional arcs, parallel with the orientation direction, that are all orders of 57.7-Å spacing; (2) a quite broad and diffuse equatorial arc, composed of two arcs with spacing of 4.5 and 4.0 Å. These data are in qualitative agreement with the mesophasic Figure 8A WAXS powder pattern of 2,6-LCPU-6 quenched in liquid N_2 from the melt. Apparently the cooling rate achieved by drawing fibers from the melt and quenching them in room temperature air is fast enough to bring the sample into the mesophase. Unfortunately we can draw very few conclusions about the mesophase structure of the 2,6-LCPU-6 from this poorly oriented WAXS fiber pattern.

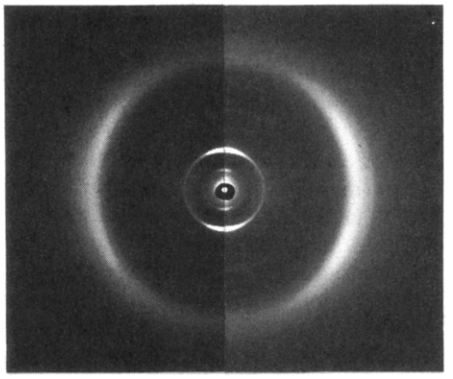

Figure 10. Room-temperature X-ray diffraction pattern of a high molecular weight 2,6-LCPU-6 fiber drawn from the melt (underexposed, left half; overexposed, right half). Fiber axis is vertical.

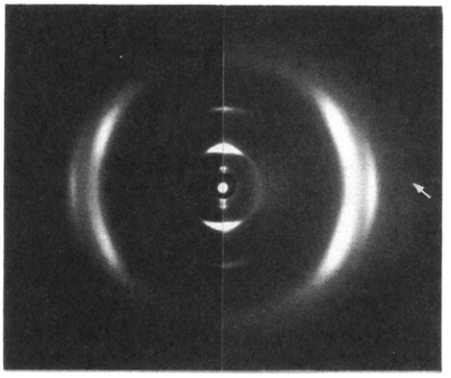

Figure 11. Room-temperature X-ray diffraction pattern of a high molecular weight 2,6-LCPU-6 fiber drawn from the melt and Soxhlet extracted in MeOH for 4 days (underexposed, left half; overexposed, right half). Fiber axis is vertical.

Frequently orientation as well as domain coarsening can be enhanced with proper thermal treatment of fibers under stress. This generally results in an increase of the phase which is stable at the annealing temperature and pressure at the expense of the other phases. The monotropic liquid crystalline nature of 2,6-LCPU-6 makes it clear that thermal treatment cannot be used to enhance the thermodynamically unstable mesophase. Obviously the task of obtaining higher orientation, with the present molecular weight sample, is equivalent to finding a way to prevent the polymer from achieving equilibrium. Plasticization with a low molecular weight compound that will provide partial mobility to allow the system to reorganize was our next attempt. Hot MeOH and room-temperature 50% DMF–50% H_2O were the two systems we tried. Even though originally we were reluctant to use the above solvents due to our experience with normal polyurethanes, where they induce crystallinity, the results were unexpectedly rewarding. Soxhlet extraction (in hot methanol for 4 days) of the fibers of Figure 10 under 0.5–3-g tension resulted in an appreciable molecular orientation, which is shown in the WAXS fiber pattern of Figure 11. Similar results were also obtained from the 50% DMF–50% H_2O mixture. The removal of DMF and H_2O was ensured by washing the treated fiber in cold MeOH for 12 h and overnight vacuum drying at 60 °C. An attempt to provide a physical insight into whatever process is involved to achieve this orientation is based on the following scenario. Plasticization occurs predominantly in the small mesophase domains which are randomly oriented along the fiber due to weaker interaction with the strong elongational flow. Deposition of the plasticized molecules on the strongly oriented larger domains thickens them, similar

to crystal annealing.

Figure 11 exhibits the same features as Figure 10, but substantially more resolved. The much sharper meridional arcs are orders of 57.8 Å, only 0.1 Å larger than those of the untreated fibers. This indicates the negligible perturbation of the original structure resulting from the hot MeOH treatment. Significant resolution enhancement is observed at the wider angles. The quite broad and diffuse equatorial arc of Figure 10 has been split into diffuse four-point, off-equatorial wide-angle reflections centered at a spacing of 4.5 Å with intensity maxima lying between the 004 and 008 layer line spacing, and a well-defined equatorial arc centered on the 4.0-Å spacing. In addition to these wide-angle reflections there is a weak and diffuse equatorial crescent, centered at 3.3 Å. The position of this crescent is indicated in Figure 11 with an arrow on the overexposed section of the pattern, where it is visible.

The 57.6–58.7 Å is almost twice the value reported for the chain-axis repeat (*c* spacing) of the related 2,4-LCPU-6.[6,10,11] This comes from the fact that previous researchers have neglected the presence of a backbone kink per monomer repeat, arising from the meta-substituted benzene ring of the 2,6-TDI, and assumed that the *c* spacing arises from one repeat only. Consequently the layer line spacings were assigned to 001, 002 (strong), and 004 reflections instead of to 002, 004 (strong), and 008 reflections. This explains the assignment difference of this publication relative to previous publications.[6,10,11] As will become obvious in the third paper of this series, the use of a fiber repeat consisting of two monomer repeat units (*dimer*) related by a 2-fold screw axis or glide plane aligned parallel to the fiber axis is essential to obtain regular molecular sequences and packing, as well as to justify the observed reflection intensities. A centrosymmetric dimer repeat can also justify the observed intensities. Unfortunately its applicability is restricted only in the disordered mesophase rather than the ordered crystalline phase where the repulsions of TDI's methyl group (from the surrounding chains) distort the dimer repeat away from centrosymmetricity.

A dimer repeat has been repeatedly observed in the literature when the backbone of the monomer is kinked, frequently due to an odd number of atoms per monomer backbone. For example, the crystalline chain-axis repeat proposed by Blackwell et al. for the 4,4′-diphenylmethane diisocyanate (MDI)–1,4-butanediol (BDO) polyurethane[17,18] consists of two repeat units. This arises from the odd methylene group on the center of the MDI unit which introduces a kink in its structure. Similar behavior is observed with the aromatic polyimide Kapton H (DuPont), synthesized from pyromellitic dianhydride and diaminodiphenyl ether,[31,32] where the ether oxygen introduces the kink. Polyaniline also displays similar behavior[33] with the nitrogen atom introducing the kink.

It is apparent that the mesophase under investigation is not one of the "classics" frequently encountered in liquid crystal textbooks.[34] The complex nature of the Figure 10 WAXS fiber pattern arises from a superposition of elements, which will be discussed extensively in the following papers of the series. Currently we will present briefly the basic molecular architecture that characterizes this system. The presence of a meta-substituted benzene ring (2,6-TDI) introduces a backbone distortion in the structure. Assuming a more or less extended hexamethylene spacer in BHHBP, the 57.6–58.2-Å repeat can be achieved by the introduction of a 54.0–54.5° tilt angle, between the planes of the TDI ring and the urethane group. This angle was determined from periodic boundary[39] energy minimization based on the Dreiding II[40] force field, conducted with the Molecular Simulations Inc., Polygraf module. The biphenol moiety orients with its plane (which contains the O···O axis) at 51° with respect to the all-trans hexamethylene plane. Based primarily on the TDI–urethane torsion angle and secondarily on the biphenyl–hexamethylene torsion angle, the fully extended 2,6-LCPU-6 dimer repeat can be over 70 Å long with only a 15% reduction in the H-bonding energy. This reduction arises primarily from the H-bonding angle (N–H···O), which for the case of 73.2-Å-long repeat is ~164°. Allowing the dimer as well as its unit cell to relax, we obtain an equilibrium repeat of 57.8 Å with H-bonding angle (N–H···O) of 176°. Future publications will address this sensitive problem extensively, with particular emphasis on the phenyl–urethane torsional barrier, which will be the backbone of the entire analysis. The crystalline structure of 2,6-LCPU-6, which will be discussed in detail in the following papers of the series, suggests the absence of qauche conformations in the hexamethylene spacer. On the basis of this result, and from the high-order mesophase structure with repeat length only 0.2–0.5 Å shorter than the crystalline repeat, the existence of gauche conformations in the "perfected" mesophase structure is unlikely but not completely ruled out.

A schematic representation of the mesophase of 2,6-LCPU-6 is illustrated in Figure 12. Biphenyls and 2,6-TDI moieties form alternative electron-dense layers perpendicular to the fiber axis. These layers along with the 2_1 screw axis or a *c*-axial glide symmetry element, result in only the even meridional reflections ($00l$: $l = 2n$) to be observed. The strong 004 meridional reflection can be explained by a mirror reflection symmetry element perpendicular to the 2,6-TDI ring and the fact that the BHHBP portions lie in the 014 plane.[29,30] Similarly the crystal structure of MDI–BDO polyurethane reported by Blackwell et al.[17,18] shows only a strong 004 reflection. The alternative tilted biphenyls lie at an approximate distance of ca. 4.5 Å from each other and give rise to the four diffuse equatorial arcs of Figure 11. Smectic C mesophases[26,27] demonstrate similar arrangements of the wide-angle diffuse arcs. The well-defined equatorial arc at 4.0 Å, and the diffuse equatorial crescent at ca. 3.3 Å, indicate an order higher than smectic C mesophase.[24,34] From the fact that these two reflections are aligned on the equator, combined with the tilted biphenyls and hexamethylene spacer, we can conclude that they arise from three-dimensional correlations of the 2,6-TDI moieties (Figure 12). This strong correlation arises from the restricted mobility of the 2,6-TDI moiety due to its meta-substituted benzene ring (backbone kink). Recently, for a side-chain poly(organophosphazene) in a smectic C state, Atkins et al.[20] reported mesophase oriented patterns which look very much like that of Figure 11, except for the outer two reflections mentioned above. The schematic diagram they used to represent the herringbone arrangement of the side-chain liquid crystal poly(organophosphazene) looks similar to that of Figure 12 with the only major difference being the backbone arrangement (parallel to smectic layers (side-chain liquid crystal)) vs perpendicular to smectic layers (main-chain liquid crystal)). According to their explanation, the lack of *hkl* reflections is due to the absent three-dimensional correlation between the smectic layers. In contrast to side-chain liquid crystals, the main-chain liquid crystal of 2,6-LCPU-6 retains this three-dimensional correlation due to bond connectivity and therefore is expected to demonstrate a higher order.

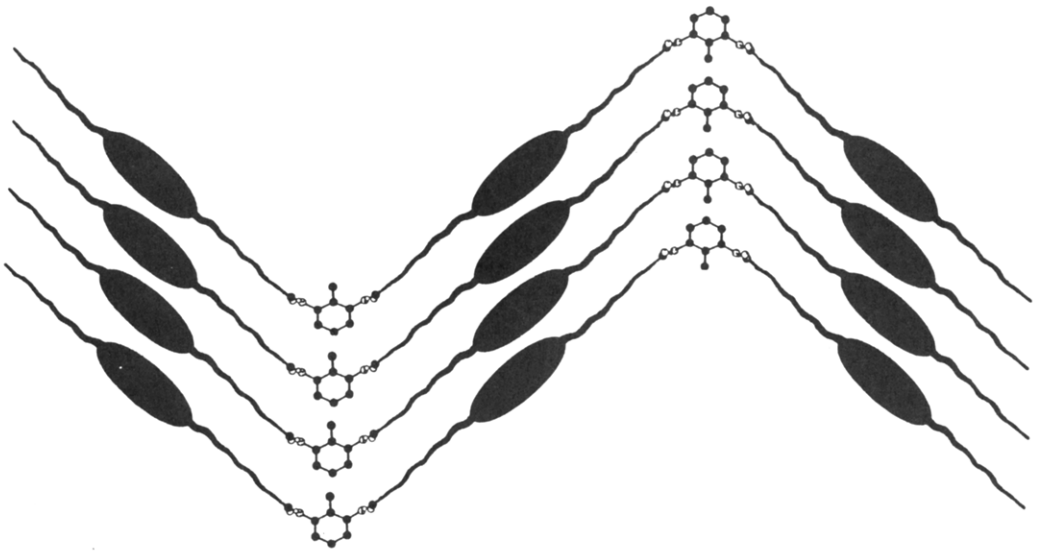

Figure 12. Schematic diagram to illustrate structural criteria needed to explain basic features of the mesophase oriented WAXS fiber pattern of Figure 11. The carbon atoms (black circles) and heteroatoms (lightly spotted white circles) portray the less mobile meta-substituted 2,6-TDI moiety. The biphenyl mesogen units (ovals) along with the hexamethylene spacer (black curly string) portray the more mobile regions. All hydrogens have been removed for clarity (See text for details). Fiber axis is horizontal.

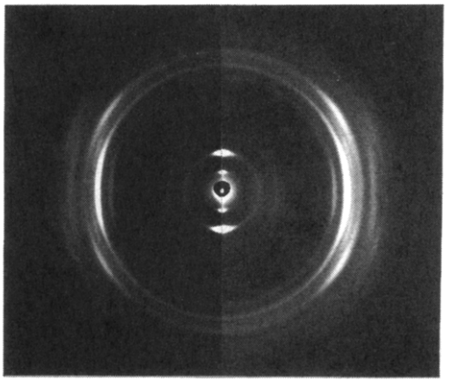

Figure 13. Room-temperature X-ray diffraction pattern of the high molecular weight 2,6-LCPU-6 fiber of Figure 11 subjected to 5-days annealing at 165 °C (underexposed, left half; overexposed, right half). Fiber axis is vertical.

Heat treatment of the well-oriented fibers above 140 °C produces highly oriented crystalline fibers. Figure 13 shows the oriented WAXS pattern of the fiber of Figure 11 subjected to 5-days annealing at 165 °C. The lattice spacings of the 17 reflections of Figure 13 are in qualitative agreement with the spacings of Figures 6 and 8C and D, indicative of the strong order in the crystal phase. The crystallographic analysis will be discussed in detail in the following papers of this series.

Optical Microscopy. Slow heating of 2,6-LCPU-6 indicates partial melting around 192 °C, followed by complete isotropization above 200 °C. Between 192 and 200 °C we observe a partial molten state which possesses adequate fluidity, with no birefringence in the fluid portion.

Upon cooling from the isotropic liquid, a fine white texture is formed at ~157 °C for the low molecular weight and 150 °C for the high molecular weight. This fine white texture persists upon reheating until 194 °C, where it starts to melt slowly as described above. The sample quenched from the melt with cold air demonstrates a fine schlieren texture.[34] Soxhlet extraction in hot MeOH coarsens considerably this schlieren texture, which is presented in Figure 14A. In addition to this, Figure 14B indicates the existence of banded spherulitic textures (pointed out by white arrows) embedded in the schlieren texture. These

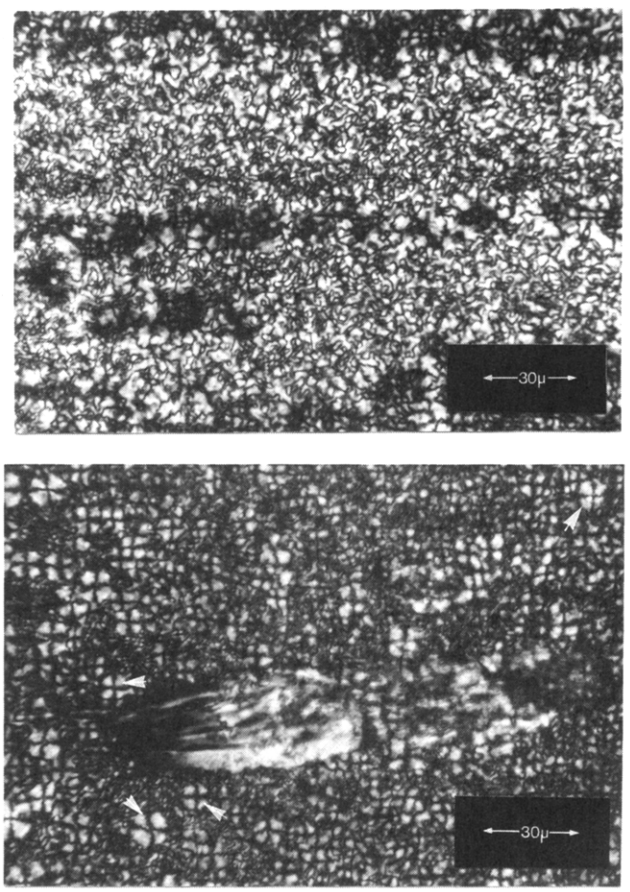

Figure 14. Room-temperature, cross-polarized optical micrographs from different regions of a 2,6-LCPU-6 sample quenched from the melt with cold air and Soxhlet extracted in hot methanol for 2 days: (A, top) the schlieren texture of the smectic mesophase; (B, bottom) the schlieren texture of the smectic mesophase along with banded spherulites (indicated with the white arrows).

spherulites were found in low quantities, gathered together in sections of the sample. Figure 14B shows an area of the sample where the spherulite concentration is relatively high while most of the sample has the appearance of Figure 14A. This is the result of a nonuniform quenching which generates regions rich in crystallinity. Soxhlet extraction

in hot methanol coarsened the schlieren texture as well as the small crystals to result in the Figure 14 textures. More uniform quenching and Soxhlet extraction resulted in lower concentrations of these spherulitic textures, while slower cooling and Soxhlet extraction resulted in higher concentrations. Slow cooling rates result in complete crystallization, which is not amenable to perfection, upon Soxhlet extraction in hot MeOH. This is due to the highly insoluble nature of the crystal domains in MeOH. Upon heating, we observe no textural changes in the vicinity of 140 °C where the mesophase to crystal transition occurs. Further heating results in the melting of the schlieren texture at ~190 °C, followed by the melting of the spherulitic texture at ~200 °C. This is in qualitative agreement with the DSC data of Figure 7, where we explained the higher melting point endotherm as melting of crystalline regions with different morphology. Smyth et al.[6] reported similar morphologies for the 2,4-LCPU-6. The spherulitic morphology was produced from the isothermal melt, and possessed very high perfection, while the threaded crystalline morphology was produced from the mesophase. We attempted numerous times with DSC and polarized optical microscopy to crystallize the 2,6-LCPU-6 from its melt, over a 35 °C region, above the crystallization temperature without success. The reason for this as well as the unusual textures shown in Figure 14B must lie in the nature of 2,6-LCPU-6 and is not known at present.

Long-term annealing of the schlieren texture of Figure 14A resulted in a substantially brighter threaded structure, which melts higher than 200 °C. This is in qualitative agreement with the annealing data of Figure 4, where the low-temperature endotherm is amenable to perfection.

It might be argued that the phase we call mesophase might arise from the presence of small disordered crystallites. However, the polarizing optical microscopic data, coupled with the X-ray scattering data (based on the relative intensitied[37,38] of Figures 10 and 11) and the detailed DSC analysis, suggest that the term mesophase is more consistent than the alternative mentioned above.

Conclusions

(1) DSC, X-ray diffraction, and polarized optical microscopic data prove unambiguously the monotropic liquid crystalline nature of the 2,6-LCPU-6. The isotropic to mesophase transition is approximately 60–70 °C lower than the crystal melting transition. This very large temperature difference, along with the regular structure of 2,6-LCPU-6, results in the mesophase being accessible only with very fast cooling rates. Cooling rates higher than 100 °C/min need to be employed in order to avoid homogeneous nucleation and crystallization and to bring the sample into the mesophase (Figure 3).

(2) X-ray diffraction patterns obtained from the frozen mesophase indicate higher order than smectic C mesophases. The layer thickness is ca. 58 Å and is found to expand slightly upon mesophase perfection. Similar expansion occurs also in the crystalline state upon perfection to a value of 58.7 Å. The zigzag structure proposed in Figure 12 is a result of the kink introduced by the meta-substituted benzene ring of the 2,6-TDI moiety. The centrosymmetric structure explains the presence of the even-order layer reflections (00*l*) as well as the strong intensity of the 004 reflection. The lateral order in the mesophase arises from the restricted mobility around the backbone kink (2,6-TDI moiety). The high order of the 2,6-LCPU-6 mesophase has been also observed by DSC.

(3) Soxhlet extraction in hot MeOH of the quenched mesophase results in considerable orientation enhancement as well as phase thickening and perfection. The value of this technique arises from its ability to perfect an unstable phase, such as the mesophase of 2,6-LCPU-6, preventing the polymer from achieving equilibrium. Using this technique, we obtained highly oriented mesophase and crystalline WAXS patterns which are the basis of the crystallographic analysis to be presented in the following papers of this series.

(4) Polarized optical microscopy studies demonstrate that 2,6-LCPU-6 exhibits two macroscopically distinct crystal morphologies—a spherulitic morphology produced from slow cooling and a threaded crystalline morphology when it crystallizes upon heating from the quenched mesophase.

Acknowledgment. We acknowledge suggestions during the course of this study from Professors K. Tashiro, E. Atkins, S. W. Kantor, and H. D. Stidham. We thank Mr. Eiji Sawa for conducting the viscosity measurements and Mr. P. J. Stenhouse for providing the high molecular weight 2,6-LCPU-6 sample. Last, but not least, we are grateful to the Center for UMass–Industry Research in Polymers (CUMIRP) and to the Army Research Office (Grant APO-23941-CH) for financial support of this research.

References and Notes

(1) Ciferri, A.; Krigbaum, W. R.; Meyer, R. B. *Polymer Liquid Crystals*; Academic Press: New York, 1982.
(2) Blumstein, A. *Liquid Crystalline Order in Polymers*; Academic Press: New York, 1978.
(3) Ober, C. K.; Bluhm, T. L. *Current Topics in Polymer Science*; Ottenbrite, R. M., Utracki, L. A., Inoue, S., Eds. 1987; Vol. 1, p 249.
(4) Dyer, E.; Hammond, R. J. *J. Polym. Sci. Part A* **1964**, *2*, 1.
(5) Yang, W. P.; Macosko, C. W.; Wellinghoff, S. T. *Polymer* **1986**, *27*, 1235.
(6) Smyth, G.; Valles, E. M.; Pollack, S. K.; Grebowicz, J.; Stenhouse, P. J.; Hsu, S. L.; MacKnight, W. J. *Macromolecules* **1990**, *23*, 3389.
(7) (a) Papadimitrakopoulos, F.; Kantor, S. W.; MacKnight, W. J. In *Recent Advances in Fiber and Polymer Science*; Fornes, R. E., Gildert, R. D., Eds.; VCH Publishers: New York, submitted. (b) Papadimitrakopoulos, F.; Kantor, S. W.; MacKnight, W. J. *Polym. Prepr. (Am. Chem. Soc., Div. Polym. Chem.)* **1990**, *31* (1), 486.
(8) (a) Mormann, W.; Brahm, M. *Macromolecules* **1991**, *24*, 1096. (b) Mormann, W.; Brahm, M. *Macromol. Chem.* **1989**, *190*, 631. (c) Lorenz, R.; Els, M.; Haulena, F.; Schmitz, A.; Lorenz, O. *Angew. Makrom. Chem.* **1990**, *180*, 51.
(9) (a) Iimura, K.; Koide, N.; Tanabe, H.; Takeda, M. *Macromol. Chem.* **1981**, *182*, 2569. (b) Tanaka, M.; Nakaya, T. *J. Macromol. Sci.-Chem. A* **1987**, *24*, 777. (c) Tanaka, M.; Nakaya, T. *Macromol. Chem.* **1986**, *187*, 2345.
(10) Pollack, S. K.; Shen, D. Y.; Hsu, S. L.; Wang, Q.; Stidham, H. D. *Macromolecules* **1989**, *22*, 551.
(11) Stenhouse, P. J.; Valles, E. M.; Kantor, S. W.; MacKnight, W. J. *Macromolecules* **1989**, *22*, 1467.
(12) Pollack, S. K.; Smyth, G.; Stenhouse, P. J.; Papadimitrakopoulos, F.; Hsu, S. L.; Kantor, S. W.; MacKnight, W. J. *Polym. Prepr. (Am. Chem. Soc., Div. Polym. Chem.)* **1989**, *30* (2), 517.
(13) Shen, D. Y.; Pollack, S. K.; Hsu, S. L. *Macromolecules* **1989**, *22*, 2564.
(14) Keller, A.; Ungar G., to be published.
(15) Percec, V.; Tomazos, D.; Pugh, C. *Macromolecules* **1989**, *22*, 3259.
(16) Tadokoro, H. *Structure of Crystalline Polymers*; Wiley-Interscience Publications: New York, 1979.
(17) Blackwell, J.; Gardner, K. H. *Polymer* **1979**, *20*, 13.
(18) Biswas, A.; Gardner, K. H.; Mojtkowski, P. W. *Polym. Prepr. (Am. Chem. Soc., Div. Polym. Chem.)* **1989**, *30* (2), 513.
(19) (a) Hong, S. K.; Blackwell, J. *Polymer* **1989**, *30*, 225. (b) Biswas, A.; Blackwell, J. *Macromolecules* **1988**, *21*, 3146, 3152, 3158.
(20) Singler, R. E.; Willingham, R. A.; Noel, C.; Friedrich, C.; Bosio, L.; Atkins, E. *Macromolecules* **1991**, *24*, 510.
(21) Nishimura, H.; OKano, T.; Sarko, A. *Macromolecules* **1991**, *24*, 759.
(22) Papadimitrakopoulos, F.; Hsu, S. L.; MacKnight, W. J., unpublished data.

(23) Shriver, D. F.; Drezdon, M. A. *The Manipulation of Air-Sensitive Compounds*, 2nd ed.; Wiley-Interscience Publications: New York, 1986.
(24) Doucet, J. *The Molecular Physics of Liquid Crystals*; Luckhurst, G. L., Gray, G. W., Eds.; Academic Press: New York, 1979; Chapter 14, p 317.
(25) Wyckoff, R. W. G. *Crystal Structures*, 2nd ed.; Interscience Publishers: New York, 1963–1965; Vol 5.
(26) Leadbetter, A. J.; Norris, E. K. *Mol. Phys.* **1979**, *38*, 669.
(27) Azaroff, L. V. *Mol. Cryst. Liq. Cryst.* **1980**, *60*, 73.
(28) Wunderlich, B. *Macromolecular Physics*; Academic Press: 1973–1980; Vols. 1–3.
(29) G. Burns, Glazer, A. M. *Space Groups for Solid State Scientists*, 2nd ed.; Academic Press: New York, 1990.
(30) Henry, N. F. M.; Lonsdale, K. *International Tables for X-Ray Crystallography*; Kynoch Press: Birmingham, England, 1969; Vol. 1.
(31) Kazaryan, L. G.; Tsvankin, D. Ya.; Ginzburg, B. M.; Tuichiev, Sh.; Korzhavin, L. N.; Frenkel, S. Ya. *Vysokomol. Soyedin.* **1972**, *A14*, 1199.
(32) Conte, G.; D'ilario, L.; Pavel, N. V.; Snamprogetti, S. A.; Giglio, E. *J. Polym. Sci., Polym. Phys. Ed.* **1976**, *14*, 1553.
(33) Pouget, J. P.; Jozefowicz, M. E.; Epstein, A. J.; Tang, X.; MacDiarmid, A. G. *Macromolecules* **1991**, *24*, 779.
(34) Gray, G. W.; Goodby, J. W. G. *Smectic Liquid Crystals, Textures and Structures*; Leonard Hill: Philadelphia, PA, 1984.
(35) Stenhouse, P. J.; Papadimitrakopoulos, F.; MacKnight, W. J., unpublished data.
(36) Leadbetter, A. J.; Norris, E. K. *Mol. Phys.* **1979**, *38*, 669.
(37) Tsukruk, V.; Shilov, V.; Lipatov, Y. *Macromolecules* **1986**, *19*, 1308.
(38) Tsukruk, V. V.; Shilov, V. V. *Polymer* **1990**, *31*, 1793.
(39) McCammon, J. A.; Harvey, S. C. *Dynamics of Proteins and Nucleic Acids*; Cambridge University Press: Cambridge, England, 1987.
(40) Mayo, S. L.; Olafson, B. D.; Goddard, W. A. *J. Phys. Chem.* **1990**, *94*, 8897.

Registry No. BHHP, 97087-90-6; (BHHP)(TDI) (copolymer), 142457-44-1.